Ceramics International 44 (2018) 17909–17913

Contents lists available at ScienceDirect

Ceramics International

journal homepage: www.elsevier.com/locate/ceramint

Effects of dopants on the microstructure and phase-purity control in PMN-PT ceramics

X. Chen[a,b,*], S. Chen[b], A. Bruner[c], R. Gaume[a,b,d]

[a] Department of Materials Science and Engineering, University of Central Florida, Orlando, FL 32816,USA
[b] College of Optics and Photonics, University of Central Florida, Orlando, FL 32816, USA
[c] Applied Physics Division, Soreq Nuclear Research Center, Yavne 81800, Israel
[d] NanoScience Technology Center, University of Central Florida, Orlando, FL 32816, USA

ARTICLE INFO

Keywords:
Transient liquid-phase sintering
Perovskite
Transparent ceramic
Sintering additive

ABSTRACT

The effects of Pb^{2+}, Ba^{2+}, La^{3+}, Y^{3+} and Gd^{3+} dopants on the densification and microstructure evolution of PMN-PT ceramics are investigated. The ceramics were reactively-sintered between 850 and 1250 °C in oxygen atmosphere. After sintering, all ceramics reached a relative density greater than 98%. XRD and SEM results revealed that lanthanum doping produces pure perovskite phase with unimodal rounded grains whereas other dopants yield microstructures with faceted grains due to the liquid phase formed in the intermediate stage. The mechanism for the observed differences in phase and morphology is also explored. The slower densification rate of La-doped samples helps maintain an open porosity network and favors the outgassing of the initial excess of PbO. The delayed densification contributes to the formation of pure perovskite at a temperature of 850 °C. Preferential A-site occupancy of La^{3+} lowers the oxygen vacancy concentration which suppresses grain growth.

1. Introduction

Solid-solutions of lead magnesium niobate and lead titanate (1-*x*)Pb($Mg_{1/3}Nb_{2/3}$)O_3-*x*$PbTiO_3$, known as PMN-PT, exhibit high dielectric permittivity, high piezoelectric coefficients and have led to varied applications as sensors and actuators [1–4]. These properties are strongly dependent on the molar fraction of lead titanate *x*, and the highest dielectric constant and piezoelectric response have been found within the so-called morphotropic phase boundary (MPB) composition range $0.3 < x < 0.35$ [5–8]. In addition, PMN-PT exhibits high electro-optic (EO) coefficients and strong photorefractive effects [9–12]. For example, Ruan *et al.* reported EO coefficients as high as 66×10^{-16} m^2/V^2 and highly transparency in La-doped 0.75PMN-0.25PT ceramics [13]. Compare to single crystal, ceramics can be easily fabricated in large scale for device applications [14,15].

Like all other lead-containing members of its family, PMN-PT ceramics produce a parasitic pyrochlore phase due to the volatility of PbO at high sintering temperatures or long sintering times. Hence, an excess of PbO is often added to compensate for this loss. This excess lead oxide also forms a liquid phase during sintering and helps the densification [16,17]. In addition, the use of dopants allow for an effective means to control grain growth in these compounds, with direct influence on their dielectric, ferroelectric, piezoelectric and EO properties [18–20]. Lanthanum-doped PMN-PT was reported to be a promising candidate for fine-grain piezoelectric [21] and for improving the transparency for the electric-optic applications [13,22–24]. However, the mechanism by which lanthanum controls grain growth and favors full densification is not fully known and this paper addresses this question by comparing the effectiveness of various dopants on grain growth control and densification in 0.75PMN-0.25PT ceramics. Gd^{3+} and Y^{3+} were chosen for comparison with La^{3+}, in order to illustrate the effect of radius on grain growth control and site occupation where both of them have the same valence as La^{3+}. Ba^{2+} was considered with reference from previous work on PLZT ceramics [25,26].

2. Experimental procedure

Lead oxide (PbO, 99.9%, Alfa Aesar), magnesium niobium oxide columbite ($MgNb_2O_6$, 99.9%, H.C. Starck) and titanium oxide (TiO_2, ≥ 99.5%, Aldrich) powders were used as starting materials for the preparation of ceramic samples with nominal composition 0.75Pb($Mg_{1/3}Nb_{2/3}$)O_3-0.25$PbTiO_3$ (0.75PMN-0.25PT). An additional 3 mol% doping was added in the form of lead oxide, barium oxide (99.99%, Aldrich), lanthanum oxide (99.99%, Alfa Aesar), yttrium oxide (99.9%, Alfa Aesar) or gadolinium oxide (99.99%, Alfa Aesar) to study the effect of these dopants on the sintering behavior of PMN-PT ceramics. The

* Corresponding author at: Department of Materials Science and Engineering, University of Central Florida, Orlando, FL 32816, USA.
E-mail address: xuan_chen_2013@knights.ucf.edu (X. Chen).

https://doi.org/10.1016/j.ceramint.2018.06.265
Received 26 May 2018; Received in revised form 27 June 2018; Accepted 29 June 2018
Available online 30 June 2018
0272-8842/

powders were mixed with ethanol and ball-milled with zirconia balls for 20 h. After ball-milling, the slurry was dried at 80 °C in an oven and the mixture was sieved through a 200-mesh screen. Pellets were pressed into shape in a stainless steel die, and subsequently cold-isostatically pressed at 200 MPa. The green-bodies were pre-sintered at 850 °C for 2 h, and followed by sintering at different temperatures (850, 950, 1050, 1150, and 1250 °C) for 4 h in pure oxygen.

The densities of sintered samples were measured by using Archimedes' method with deionized water as the immersion medium. The phase composition of the sintered ceramics was determined by X-ray diffraction (XRD) (PANalytical Empyrean), whereas their microstructures were observed by scanning electron microscopy (SEM) (Zeiss, Ultra-55). The grain sizes were measured by the linear intercept method (more than 200 grains counted) using ImageJ (National Institute of Health) from the SEM images. The SEM microstructures were obtained on unpolished ceramics in order to prevent damage and the contamination by abrasives of porous samples.

3. Results and discussion

3.1. Transient liquid-phase sintering

Using the synthesis conditions described above, the phase content of the doped pellets was followed by x-ray diffraction after sintering (Fig. 1). Ba-doped samples show the same phenomenon as the Pb-doped samples at different sintering temperatures. A well-annealed platinum foil, placed on the surface of the samples, was used as an internal standard for these measurements, and the x-ray analysis was performed on the patterns corrected for any instrumental shift. As expected, all samples show that the initial excess of PbO evaporates during sintering, and that, at a temperature of 1150 °C and for a sintering time of 4 h, the PMN-PT perovskite phase is the only remaining phase. However, excessive evaporation can lead to perovskite decomposition and the formation of columbite, as in the case of Y-doped PMN-PT samples held at 1250 °C for 4 h. The case of La-doped samples is peculiar as phase-pure PMN-PT is obtained regardless of the sintering temperature. In the intermediate stage, all samples, with the exception of the La-doped ones, form a liquid phase as a result of excess PbO [27,28]. During sintering, the capillary force induced by the liquid phase on the solid particles contributes to densification and this may be the reason why densification proceeds at a lower temperature with these dopants (Fig. 2). On the other hand, the slow densification rate of La-doped samples helps maintain an open porosity network for a longer time and favors the outgassing of the initial excess of PbO. The delayed densification contributes to the formation of phase pure PMN-PT at a temperature as low as 850 °C. At 1250 °C, all compositions reach final relative densities greater than 98%.

3.2. Microstructure evolution

It is well known that the presence of a liquid phase influences the ceramic microstructure by affecting not only the size but also the shape of the grains. Fig. 3 shows SEM images of the ceramic microstructures for the various dopants and sintering temperatures selected in this study. As can be seen on these pictures, all dopants, with the notable exception of lanthanum, produce faceted grains. Both Ba^{2+} and Pb^{2+}-doped samples exhibit the same microstructure evolution between 850 and 1250 °C. In the case of Y^{3+} and Gd^{3+} doping, faceted grains appear at 1050 °C. This implies that, for these dopants, nonstationary grain-growth conditions govern the development of the microstructure, and that the ratio of the step free-energy, σ_s, which is the energy per unit length of the edge of a nucleus formed on a flat surface to the step height, h, exceeds the solid-liquid interfacial energy, γ_{sl}, [29]

$$\frac{\sigma_s}{h} > \gamma_{sl}$$

Abnormal grain-growth typically proceeds as a result of the formation of these faceted crystallites. Different with other doped samples, La-doped PMN-PT did not present a liquid phase during sintering and then the mechanism shown here is not satisfied. One potential explanation is that the solid-vapor interfacial energy for La-doped samples, which is larger than the solid-liquid interfacial energy under good surface wetting conditions in normal case, dominates the step free-energy. This helps produce a uniform grain-size distribution throughout the densification process, eventually leading to the complete removal of porosity and enhanced transparency of the samples.

3.3. Tolerance factors and dopant site occupancy considerations

In addition to the effect of the liquid phase discussed above, charge compensation mechanisms resulting from specific dopant site occupancy are likely controlling grain growth after the liquid phase disappears. The dopants' valence state and their site occupation influence the oxygen vacancy concentration, the diffusion of species and thereby the grain boundary mobilities. At ambient temperature, the 0.75PMN-0.25PT composition crystallizes into a ABO_3 rhombohedral perovskite structure. Pb^{2+} occupies the 12-fold coordinated A site and Mg^{2+}, Nb^{5+}, Ti^{4+} occupy the 6-fold coordinated B site [30]. The rhombohedral structure is considered as a pseudo-cubic structure [31]. In an ideal cubic perovskite, the ionic radii, r_i ($i = A, B, O$), satisfy the relation: $r_A + r_O = \sqrt{2}(r_B + r_O)$ [32]. The Goldschmidt tolerance factor for perovskite is defined by

$$t = \frac{r_A + r_O}{\sqrt{2}(r_B + r_O)} \quad (1)$$

Using the radii of Pb^{2+}, O^{2-} and the weighted average B-site radius for 0.75PMN-0.25PT, the ideal tolerance factor of 0.75PMN-0.25PT is $t = 0.997$. When doped, the site occupancy in the structure is controlled by the nature of the dopant ions [33]. The site occupation behavior cannot solely be determined by the tolerance factor but one should also take the strain (and its anisotropy) and distribution effects [34,35]. However, when comparing ions with similar valence state, this factor can show useful trends [36]. Here, we define t_A and t_B as the tolerance factors of a perovskite unit cell for a 3 at% cationic substitution on the A and B sites respectively, taking into account the correct coordination number.

$$t_A = \frac{0.03r + 0.97 \times r_A + r_O}{\sqrt{2}(r_B + r_O)} \quad (2)$$

$$t_B = \frac{r_A + r_O}{\sqrt{2}(0.97 \times r_B + 0.03r + r_O)} \quad (3)$$

where r stands for the radius of the substituting cation. Assuming the local strain is similar in A and B site, it is expected that if the incorporation into one site results in a tolerance factor much closer to 1 than the incorporation into the other site, then the first one would be preferred over the second. Fig. 4 shows the evolution of the tolerance factors t_A and t_B for lanthanide (Ln^{3+}) ion doping depending on their substitution site (i.e. their coordination number, CN). The ionic radius, $r(Ln^{3+}_{CN})$, ranges from 0.848 to 1.061 Å for Lu^{3+} and La^{3+}, respectively. The crossover point corresponds to a radius of 1 Å, meaning that large ions ($r(R^{3+}_{VI}) > 1$Å) prefer to occupy the A site, while small ions ($r(R^{3+}_{VI}) < 1$Å) prefer to occupy B site. Table 1

For these two cases, we consider the following two alternative incorporation reactions:

$$M_2O_3 \xrightarrow[4ABO_3]{} 2M_A^{\bullet} + O_i^{''} + 2AO \quad (4)$$

$$M_2O_3 \xrightarrow[4ABO_3]{} 2M_B^{\prime} + V_O^{\bullet\bullet} + 2BO_2 \quad (5)$$

A stands for Pb^{2+}, B stands for the effective $(Mg_{1/4}Nb_{1/2}Ti_{1/4})^{4+}$ site and M stands for the dopant ions. For ionic radii $r > 1$ Å, the ion (La^{3+}) occupy the A-site preferentially. As lanthanum goes into the A-

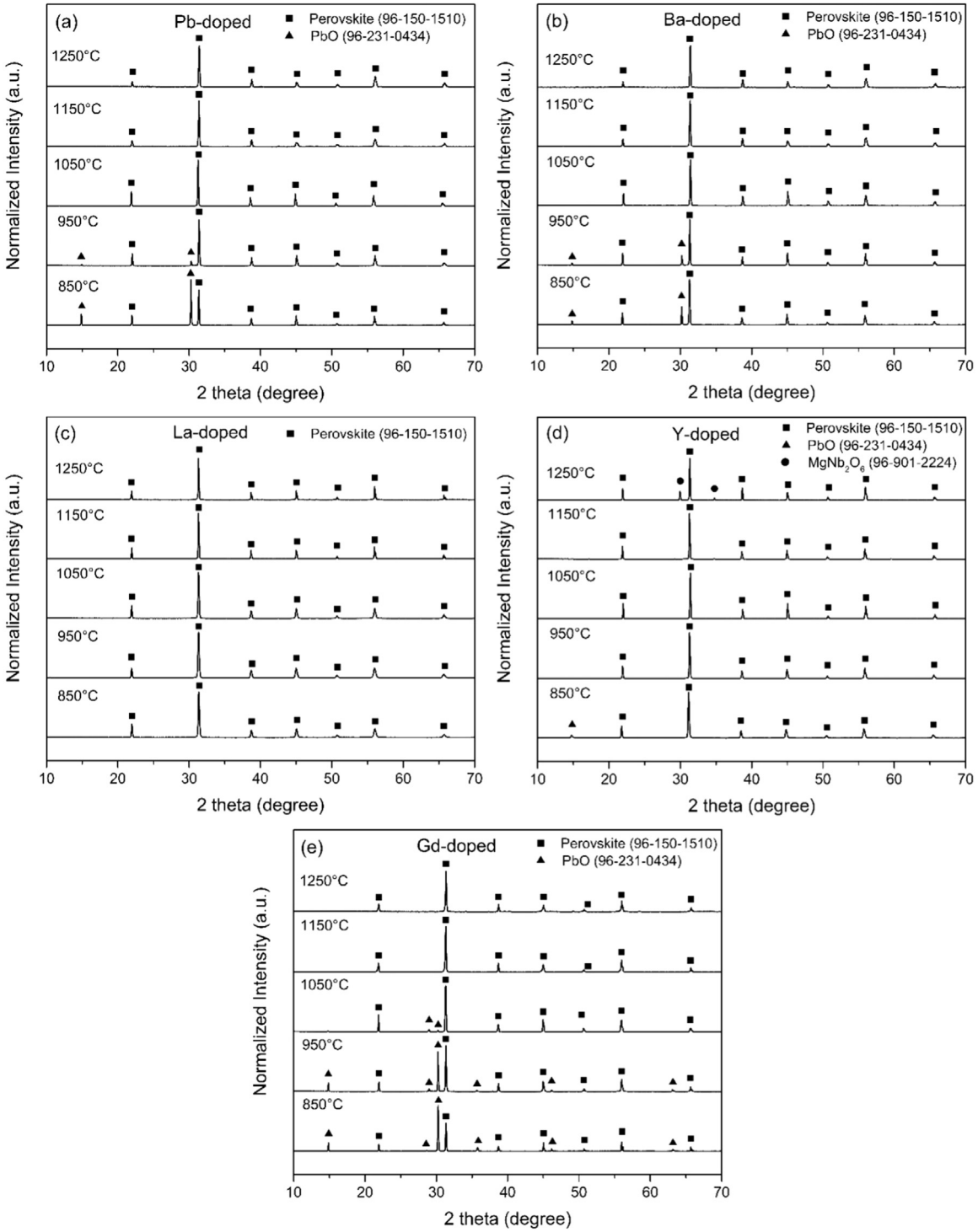

Fig. 1. X-ray diffraction patterns of 0.75PMN-0.25PT ceramic samples doped with (a) Pb^{2+}, (b) Ba^{2+}, (c) La^{3+}, (d) Y^{3+} and (e) Gd^{3+}.

site, pre-existing oxygen vacancies are consumed, which leads to a lower oxygen vacancy concentration compared to Gd^{3+}-doped and Y^{3+}-doped samples. This lower oxygen vacancy concentration decreases the diffusion rates and the mobility of grain-boundaries, as supported by our grain-growth data (Fig. 5) and similar work on La-doped PMN-PT [38]. For ionic radii $r < 1$ Å, the ions (Y^{3+} and Gd^{3+}) tend to occupy the B-site, which leads to larger oxygen vacancy concentration according to Eq. (5). This result corroborates similar findings in $BaTiO_3$ [33]. This proposed mechanism accounting for the formation of oxygen vacancies when cationic substitution operates on the B-site sublattice will however require further experimental and computational validation.

4. Conclusions

In this work, we showed the microstructure and phase evolution of PMN-PT ceramics sintered with different dopants. We have shown that La-doped PMN-PT samples do not form a liquid phase during sintering which helps the formation of a pure perovskite phase and unimodal rounded grains while samples with other dopants exhibit faceted grains. We found that the preferential A-site occupancy of La^{3+} resulting from

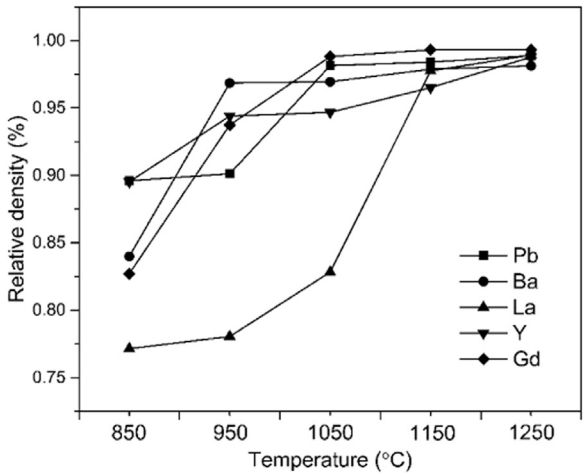

Fig. 2. Densification behavior of 0.75PMN-0.25PT ceramic samples as a function of sintering temperature for the different dopants studied in this work.

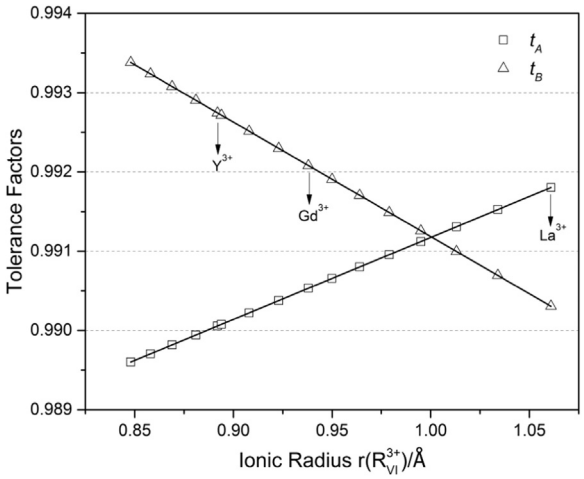

Fig. 4. The tolerance factors t_A and t_B for substation of trivalent ions on the A- and B- sites, as functions of the ionic radius.

its larger ionic radius lowers the oxygen vacancy concentration. As a result, grain growth is suppressed compared to samples doped with the smaller Y^{3+} and Gd^{3+} ions.

Acknowledgements

The authors would like to thank the Israeli Ministry of Defense for support through contract # 100254098.

Table 1
Coordination-dependent ionic radii for the dopants used in this study [37].

Dopants	Ionic Radii (Å)	
	$r_{CN\text{-}VI}$	$r_{CN\text{-}XII}$
Ba^{2+}	1.360	1.600
Pb^{2+}	1.180	1.490
La^{3+}	1.061	1.320
Gd^{3+}	0.938	1.246
Y^{3+}	0.892	1.220

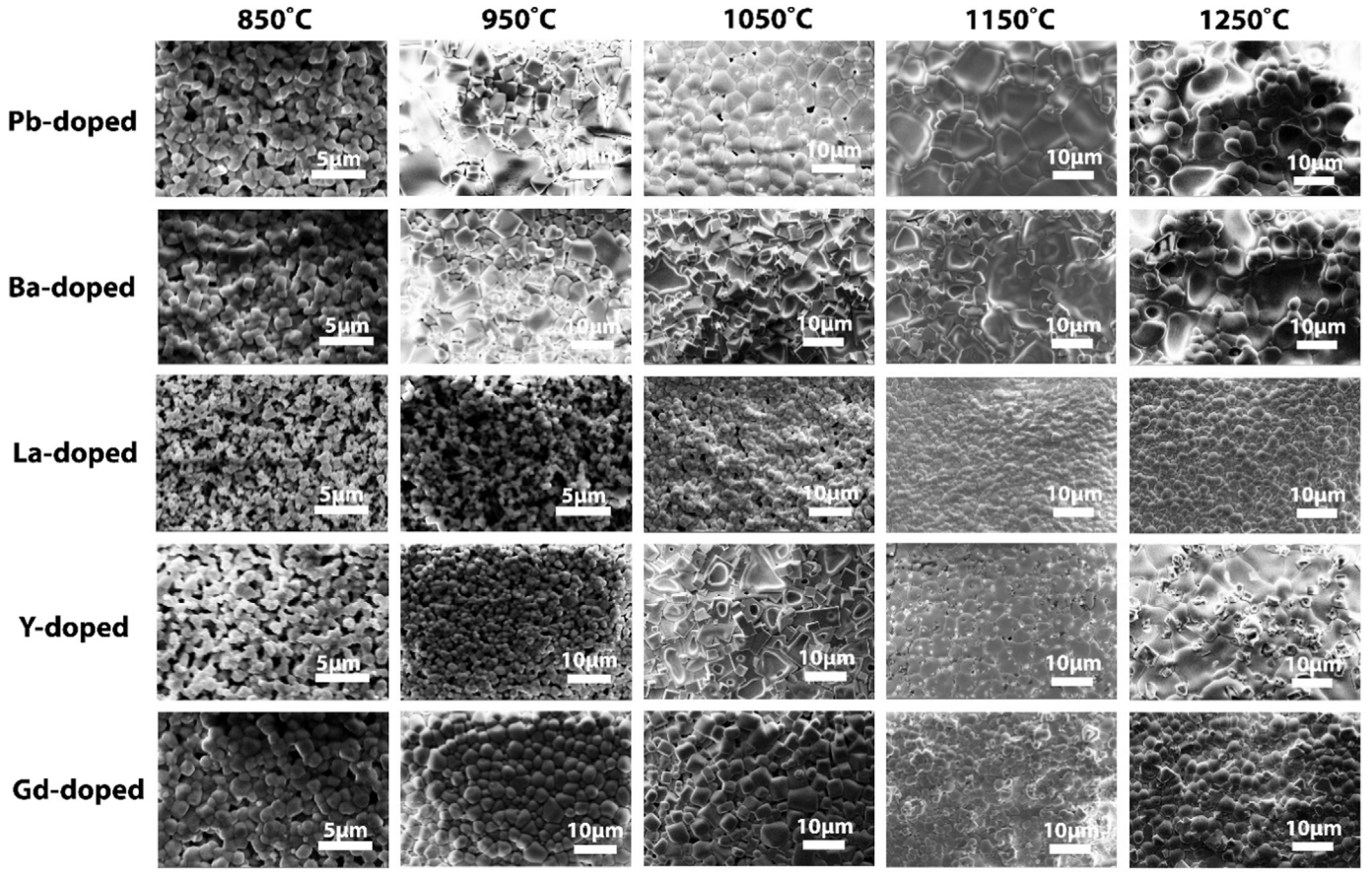

Fig. 3. Scanning Electron Microscopy images of samples with different dopants sintered at 850 °C, 950 °C, 1050 °C, 1150 °C and 1250 °C.

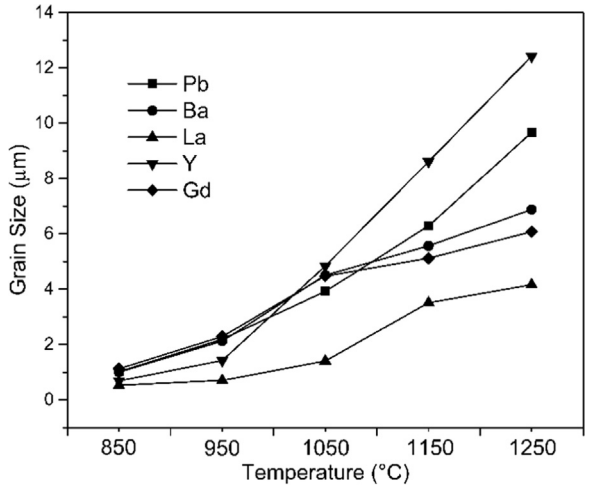

Fig. 5. Grain growth behavior of 0.75PMN-0.25PT samples with different dopants sintered at different temperatures for 4 h in oxygen.

References

[1] G.H. Haertling, Ferroelectric ceramics: history and technology, J. Am. Ceram. Soc. 82 (1999) 797–818.

[2] S. Zhao, Q. Li, Y. Feng, C. Nan, Microstructure and dielectric properties of PMN–PT ceramics prepared by the molten salts method, J. Phys. Chem. Solids 70 (2009) 639–644.

[3] P. Kumar, C. Prakash, O. Thakur, R. Chatterjee, T. Goel, Dielectric, ferroelectric and pyroelectric properties of PMNT ceramics, Phys. B: Condens. Matter 371 (2006) 313–316.

[4] J.-H. Chen, Y.-C. Liou, 0.9Pb($Mg_{1/3}Nb_{2/3}$)O_3–0.1$PbTiO_3$ relaxor ferroelectric ceramics produced by a simplified columbite route and a reaction-sintering process, Ceram. Int. 30 (2004) 157–162.

[5] T.R. Shrout, Z.P. Chang, N. Kim, S. Markgraf, Dielectric behavior of single crystals near the (1 − x) Pb($Mg_{1/3}Nb_{2/3}$)O_3-(x) $PbTiO_3$ morphotropic phase boundary, Ferroelectr. Lett. Sect. 12 (1990) 63–69.

[6] S. Choi, T.R. Shrout, S. Jang, A. Bhalla, Morphotropic phase boundary in Pb($Mg_{1/3}Nb_{2/3}$)O_3-$PbTiO_3$ system, Mater. Lett. 8 (1989) 253–255.

[7] J. Ho, K. Liu, I. Lin, Study of ferroelectricity in the PMN-PT system near the morphotropic phase boundary, J. Mater. Sci. 28 (1993) 4497–4502.

[8] M. Lejeune, J. Boilot, Low firing dielectrics based on lead magnesium niobate, Mater. Res. Bull. 20 (1985) 493–499.

[9] Y. Lu, J. Zheng, M. Croning Golomb, F. Wang, H. Jiang, J. Zhao, In-plane electro-optic anisotropy of (1 − x)Pb($Mg_{1/3}Nb_{2/3}$) O_3–x$PbTiO_3$ thin films grown on (100)-cut $LaAlO_3$, Appl. Phys. Lett. 74 (1999) 3764–3766.

[10] K. Chan, W. Tsang, C. Mak, K. Wong, Optical studies of 0.65 $PbMg_{1/3}Nb_{2/3}O_3$–0.35 $PbTiO_3$ thin films, J. Eur. Ceram. Soc. 25 (2005) 2313–2317.

[11] X. Tong, K. Lin, D. Lv, M. Yang, Z. Liu, D. Zhang, Optical properties of PMN–PT thin films prepared using pulsed laser deposition, Appl. Surf. Sci. 255 (2009) 7995–7998.

[12] H. Jiang, Y. Zou, Q. Chen, K. Li, R. Zhang, Y. Wang, H. Ming, Z. Zheng, Transparent electro-optic ceramics and devices, photonics Asia 2004, Int. Soc. Opt. Photonics (2005) 380–394.

[13] W. Ruan, G. Li, J. Zeng, J. Bian, L.S. Kamzina, H. Zeng, L. Zheng, A. Ding, Large electro-optic effect in La-doped 0.75Pb($Mg_{1/3}Nb_{2/3}$)O_3–0.25$PbTiO_3$ transparent ceramic by two-stage sintering, J. Am. Ceram. Soc. 93 (2010) 2128–2131.

[14] M.C. Shin, S.J. Chung, S.-G. Lee, R.S. Feigelson, Growth and observation of domain structure of lead magnesium niobate–lead titanate single crystals, J. Cryst. Growth 263 (2004) 412–420.

[15] L. Lim, M. Shanthi, K.K. Rajan, C. Lim, Flux growth of high-homogeneity PMN–PT single crystals and their property characterization, J. Cryst. Growth 282 (2005) 330–342.

[16] T. Frueh, E.R. Kupp, C. Compson, J. Atria, G.L. Messing, The effects of Na_2O and SiO_2 on liquid phase sintering of bayer Al_2O_3, J. Am. Ceram. Soc. 99 (2016) 2267–2272.

[17] G. Zhilun, L. Longtu, G. Suhua, Z. Xiaowen, Low-temperature sintering of lead--based piezoelectric ceramics, J. Am. Ceram. Soc. 72 (1989) 486–491.

[18] Z. Xie, M. Lugovy, N. Orlovskaya, T. Graule, J. Kuebler, M. Mueller, H. Gao, M. Radovic, D.A. Cullen, Hexagonal OsB_2: sintering, microstructure and mechanical properties, J. Alloy. Compd. 634 (2015) 168–178.

[19] Y.-H. Chen, K. Uchino, D. Viehland, Substituent effects in 0.65Pb($Mg_{1/3}Nb_{2/3}$)O_3-0.35$PbTiO_3$ piezoelectric ceramics, J. Electroceram. 6 (2001) 13–19.

[20] S.H. Lee, E.R. Kupp, A.J. Stevenson, J.M. Anderson, G.L. Messing, X. Li, E.C. Dickey, J.Q. Dumm, V.K. Simonaitis-Castillo, G.J. Quarles, Hot isostatic pressing of transparent Nd: YAG ceramics, J. Am. Ceram. Soc. 92 (2009) 1456–1463.

[21] N. Kim, W. Huebner, S.-J. Jang, T.R. Shrout, Dielectric and piezoelectric properties of lanthanum-modified lead magnesium niobium-lead titanate ceramics, Ferroelectrics 93 (1989) 341–349.

[22] W. Ji, X. He, W. Cheng, P. Qiu, X. Zeng, B. Xia, D. Wang, Effect of La content on dielectric, ferroelectric and electro-optic properties of Pb($Mg_{1/3}Nb_{2/3}$)O_3–$PbTiO_3$ transparent ceramics, Ceram. Int. 41 (2015) 1950–1956.

[23] X. Chen, S. Chen, P.-M. Clequin, W.T. Shoulders, R. Gaume, Combustion synthesis of lead oxide nanopowders for the preparation of PMN–PT transparent ceramics, Ceram. Int. 41 (2015) 755–760.

[24] K. Zhao, W. Ruan, H. Zeng, J. Zeng, G. Li, Q. Yin, Domain dynamics of La-doped PMN-PT transparent ceramics studied by piezoresponse force microscope, Appl. Surf. Sci. 293 (2014) 366–370.

[25] K. Ramam, V. Miguel, Microstructure, dielectric and ferroelectric characterization of Ba doped PLZT ceramics, Eur. Phys. J.-Appl. Phys. 35 (2006) 43–47.

[26] R. Koduri, L.S. Hermosilla, Effect of Ba on ferroelectric and piezoelectric properties of the PLZT (1.2/55/45) system, Phys. Status Solidi 203 (2006) 2119–2127.

[27] J.S. Wallace, J.M. Huh, J.E. Blendell, C.A. Handwerker, Grain growth and twin formation in 0.74 PMN·0.26 PT, J. Am. Ceram. Soc. 85 (2002) 1581–1584.

[28] L. Kong, J. Ma, W. Zhu, O. Tan, Translucent PMN and PMN-PT ceramics from high-energy ball milling derived powders, Mater. Res. Bull. 37 (2002) 23–32.

[29] Z.Z. Fang, Sintering of Advanced Materials, Elsevier, Cambridge, UK, 2010.

[30] Y. Guo, H. Luo, D. Ling, H. Xu, T. He, Z. Yin, The phase transition sequence and the location of the morphotropic phase boundary region in (1 − x)[Pb($Mg_{1/3}Nb_{2/3}$)O_3]–x$PbTiO_3$ single crystal, J. Phys.: Condens. Matter 15 (2003) L77.

[31] H. King, S. Ferguson, D. Waechter, S. Prasad, X-ray diffraction study of PMN-PT ceramics in the region of the relaxor transition, Proc. 2nd. Canada-Us CanSmart Workshop on Smart Materials and Structures, Citeseer, 2002, pp. 11–20.

[32] R.S. Roth, Classification of perovskite and other ABO_3-type compounds, J. Res. Nat. Bur. Stand 58 (1957) 75–88.

[33] Y. Tsur, T.D. Dunbar, C.A. Randall, Crystal and defect chemistry of rare earth cations in $BaTiO_3$, J. Electroceram. 7 (2001) 25–34.

[34] S.-T. Zhang, A.B. Kounga, E. Aulbach, T. Granzow, W. Jo, H.-J. Kleebe, J. Rödel, Lead-free piezoceramics with giant strain in the system $Bi_{0.5}Na_{0.5}TiO_3$–$BaTiO_3$–$K_{0.5}Na_{0.5}NbO_3$. I. Structure and room temperature properties, J. Appl. Phys. 103 (2008) 034108.

[35] B. Jaffe, Piezoelectric Ceramics, Elsevier, New York, USA, 2012.

[36] J. Sun, G. Rao, J. Liang, Crystal structure and electronic transport property of perovskite manganese oxides with a fixed tolerance factor, Appl. Phys. Lett. 70 (1997) 1900–1902.

[37] R.T. Shannon, C.T. Prewitt, Effective ionic radii in oxides and fluorides, Acta Crystallogr. Sect. B: Struct. Crystallogr. Cryst. Chem. 25 (1969) 925–946.

[38] J. Zhang, Y. Zhang, C. Lu, W. Ye, J. Su, Effect of La-doping content on the dielectric and ferroelectric properties of 0.88 Pb($Mg_{1/3}Nb_{2/3}$)O_3–0.12 $PbTiO_3$ ceramics, J. Mater. Sci.: Mater. Electron. 25 (2014) 653–658.